

Article

# A Terahertz-Microfluidic Chip with a Few Arrays of Asymmetric Meta-Atoms for the Ultra-Trace Sensing of Solutions

Kazunori Serita \*, Hironaru Murakami, Iwao Kawayama and Masayoshi Tonouchi

Institute of Laser Engineering, Osaka University, 2-6 Yamadaoka, Suita, Osaka 565-0871, Japan; hiro@ile.osaka-u.ac.jp (H.M.); kawayama@ile.osaka-u.ac.jp (I.K.); tonouchi@ile.osaka-u.ac.jp (M.T.)

\* Correspondence: serita-k@ile.osaka-u.ac.jp; Tel.: +81-6-6879-7983

Received: 15 December 2018; Accepted: 24 January 2019; Published: 30 January 2019



**Abstract:** Biosensing with terahertz (THz) waves has received large amounts of attention due to its potential to detect the functional expression of biomolecules in a label-free fashion. However, many practical challenges against the diffraction limit of THz waves and the strong absorption of THz waves into polar solvents still remain in the development of compact biosensors. Here, we present a non-linear, optical, crystal-based THz-microfluidic chip with a few arrays of asymmetric meta-atoms, an elementary unit of metamaterials, for the measurement of trace amounts of solution samples. A near-field THz emission source, that is locally generated in the process of optical rectification at a fs (femtosecond) laser irradiation spot, induces a sharp Fano resonance and modifies the resonance frequency of the meta-atoms when the channel is filled with solution samples of different concentrations. Using this chip, we successfully detected minute changes in the concentration of trace amounts of mineral water and aqueous sugar solutions by monitoring the shift in the resonance frequency. A higher detectable sensitivity of 1.4 fmol of solute in a 128 pL volume of solution was achieved. This was an improvement of one order of magnitude in the sensitivity compared to our previous experiment.

**Keywords:** terahertz; meta-atom; microfluidics; non-linear optical crystal; Fano resonance

## 1. Introduction

Microfluidics are well known to be promising tools for medical diagnoses and chemical analyses [1,2]. Their benefits include reduced sample volumes, high sensitivity, low cost, portability, and the potential to be highly integrated into micro-total analysis systems ( $\mu$ TAS). Significant progress has been made in cellular and nucleic acid studies using highly sensitive analytical techniques such as microchip electrophoresis, enzyme-linked immunosorbent assay, electrochemical quartz crystal microbalance, and surface plasmon resonance sensors with only a drop of a solution sample [3–6].

The advantageous properties of biosensing with terahertz (0.1–10 THz) waves, such as the possibility of the non-invasive detection of the picosecond dynamics of biomolecules in a label-free fashion, have also received large amounts of attention. Because such dynamics correspond to comparatively lower energy than that of infrared absorption, THz spectroscopy and imaging are powerful tools to observe new physical properties attributed to the functional expression and conformational change of biomolecules [7–12]. The combination of such THz and microfluidic technologies could result in new analytical methods capable of shortening the time required for analytical processes. However, it is difficult to perform ultra-trace measurements with THz waves, due to the spatial resolution of far-field THz waves and their strong absorption into polar solvents.

Several highly sensitive biosensing techniques with THz waves have been reported, including the detection of viruses [13], bacteria [14,15], living cells [16,17], and DNA sensors [18,19]; however, most of

these techniques focus on the use of far-field THz waves. Therefore, the macroscopic information concerning the sample is obtained, rather than the sample itself. Conversely, a laser THz emission microscope (LTEM) is a powerful tool for the measurement of samples on the sub-wavelength scale. Unlike conventional THz measurement techniques, the resolution in the LTEM is not limited by the THz waves, but by that of the optical laser source. Therefore, direct sensitive and quantitative measurements of various types of samples have been achieved [20–28]. Recently, our group applied this technique to an ultra-trace measurement of a solution and proposed a non-linear optical crystal (NLOC)-based THz-microfluidic chip with a few arrays of split-ring resonators (SRRs). The chip operates on the basis of the near-field coupling between the SRRs and the local emission of a point-like THz source that is generated in the process of optical rectification in the NLOC at the sub-wavelength scale. The liquid solution flowing into the microchannel modifies the resonance frequency in the THz transmission spectra, and we can detect femtomolar levels of solute in sub-nanoliter amounts of liquid solutions [29]. However, the meta-structures have not yet been optimized and the sensitivity can be improved by using other meta-surfaces. One of the candidate structures to obtain a better resonance response is based on the breaking of its symmetries. There are many studies of such structures using far-field THz wave excitation, however, few reports are available using near-field THz wave excitation. This knowledge could be useful for the development of a highly sensitive NLOC-based THz chip. Therefore, in this study, to further enhance the sensitivity of the THz chip, we proposed and developed a THz-microfluidic chip with asymmetric SRRs and evaluated its sensitivity using ultra-trace amounts of solutions.

## 2. Terahertz-Microfluidic Chip

Figure 1a shows a schematic drawing of the NLOC-based THz-microfluidic chip. The chip consists of a single microchannel and a few arrays of the meta-atoms, the elementary unit of the metamaterials, which are fabricated on a 500- $\mu\text{m}$ -thick, (110)-oriented gallium arsenide (GaAs) wafer. A two-gap split-ring resonator, which has a diameter of 84  $\mu\text{m}$  with gaps of 20  $\mu\text{m}$  and a linewidth of 10  $\mu\text{m}$ , was employed as the unit cell of the meta-atom, and the upper gap was shifted by “ $d$ ” = 20  $\mu\text{m}$  from the central vertical axis, as shown in the inset of Figure 1a. This structure was periodically arrayed, with a period of 100  $\mu\text{m}$  and the number of units being  $5 \times 5$  (corresponding to an area of 540  $\mu\text{m} \times 540 \mu\text{m}$ ), using a conventional photolithographic technique, followed by the deposition of 200 nm of gold after sputtering a 1-nm-thick adhesion layer of titanium. These parameters were chosen so that the meta-atoms exhibited a Fano resonance at 0.35 THz and a quadruple resonance at 0.75 THz in their THz transmittance spectra, as shown in Figure 1c,d, respectively; these resonances are associated with an anti-parallel current flow along the meta-atoms [30]. A single microchannel with a width of 16  $\mu\text{m}$ , a depth of 10  $\mu\text{m}$ , and a length of 2.2 mm was then fabricated along the space using a wet etching process. For the measurement, we used a near-field THz emission spectroscopy system that is similar to a conventional THz time-domain spectroscopy (THz-TDS) system using a fiber-coupled femtosecond (fs) laser source at a wavelength of 1560 nm [23]. The optical pump beam was focused on the central region of the central meta-atom, and THz waves were generated via the process of optical rectification at the irradiation spot with  $\phi 10 \mu\text{m}$ . In this method, after the excitation of the central meta-atom, the THz electric field is coupled to the neighboring meta-atoms on a picosecond time scale and eventually, resonance is obtained in the spectrum, as in conventional far-field THz-TDS. In our previous study, it was found that a resonance response with a sufficient Q factor was obtained when the number and period of the meta-atoms were  $5 \times 5$  units and less than 120  $\mu\text{m}$ , respectively [31]. The microchannel was fabricated near the THz source and is influenced by the coupling of the THz electric field. Therefore, the chip can determine the solution concentrations via the shift in the resonance frequency of the spectrum. A bowtie-shaped photoconductive antenna was used as a detector. Note that the system is equipped with a galvanometer, which enabled us to scan the pump laser beam to adjust the beam irradiation spot to an exact position, by monitoring the reflected laser image before the measurement. To evaluate the chip performance, the THz transmittance  $T(\omega) = E_{\text{samp}}(\omega)/E_{\text{ref}}(\omega)$

was observed, where  $E_{\text{samp}}(\omega)$  and  $E_{\text{ref}}(\omega)$  are the frequency-dependent THz amplitudes when the microchannel is filled with and without solution samples, respectively.

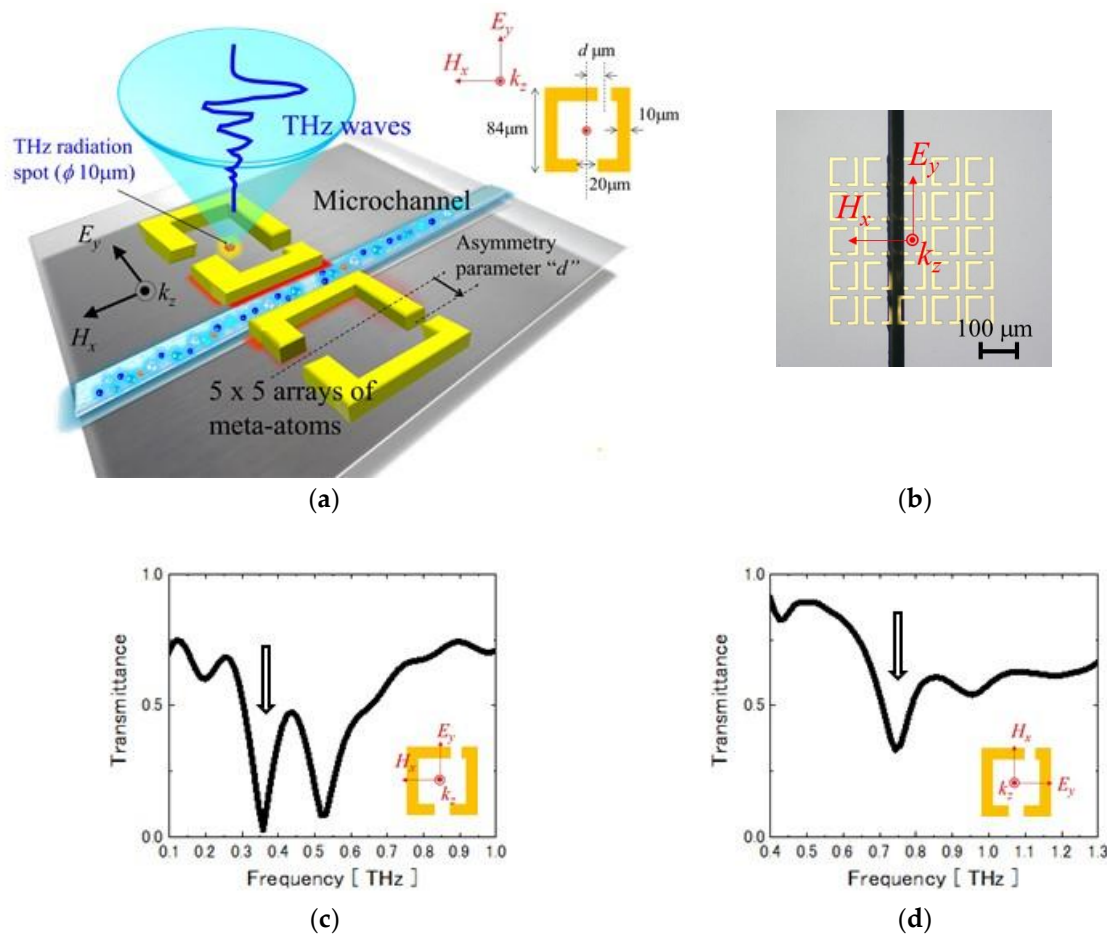


**Figure 1.** (a) A schematic drawing and (b) an optical image of the terahertz (THz) microfluidic chip. (c,d) The simulated THz transmittance spectra of the Fano and quadrupole resonances, respectively.

In conventional THz metamaterial studies of such Fano and quadrupole resonances, far-field THz waves are focused on a few thousand resonators. Therefore, the resonance response is primarily affected by the shape of each resonator [32]. Conversely, meta-atoms excited via the near-field emission of THz waves have not yet been investigated. We have previously reported typical LC (resonant circuit) resonance responses using single- and double-gap resonators [29,31], however, the case of asymmetric resonators is still incompletely understood; therefore, it is necessary to understand how the symmetry of the meta-atoms affects the resonance response. Here, we prepared two-gap meta-atoms, starting from a perfectly symmetrical one ( $d = 0$ ) and then gradually displacing the upper gap by a distance ( $d$ ) of 5 μm, 10 μm, and 20 μm while keeping the lower gap fixed. The period and the number of meta-atoms were fixed to 100 μm and  $5 \times 5$  units, respectively. Figure 2a shows the measured transmittance spectra of a perfectly symmetrical ( $d = 0$ ) meta-atom and asymmetrical meta-atoms with  $d = 5$  μm, 10 μm, and 20 μm when the pump laser beam is polarized perpendicular to the gap of the meta-atoms. One single broad resonance at approximately 0.5 THz was observed for the case of  $d = 0$ , and this resonance gradually divided into two resonances with an increasing  $d$ ; finally, clear resonances at approximately 0.4 THz and 0.55 THz were observed for both  $d = 10$  μm and 20 μm. These sharp resonances correspond to the Fano resonance, due to the symmetry breaking within the meta-atoms [30,33]. This tendency agrees with our numerical calculations (FDTD solution: Lumerical Solutions, Inc.), as shown in Figure 2b. We repeated the process for the quadrupole resonance,

by setting the polarization of the excitation laser beam parallel to the gap of the meta-atoms, and measured the THz transmittance spectra shown in Figure 2c. We observed a single resonance at 0.95 THz for the case of  $d = 0 \mu\text{m}$  but two resonances for  $d = 10 \mu\text{m}$  and  $20 \mu\text{m}$ , which agreed well with the numerical calculations, as shown in Figure 2d. The Q factors of the Fano and quadrupole resonances in this measurement were 6.5 and 10.5, respectively. These values are more than two times better than those of our previous study using symmetric meta-atoms [29]. As a result, we confirmed that asymmetric meta-atoms can be used in the near-field emission method and can support higher-Q resonance responses.

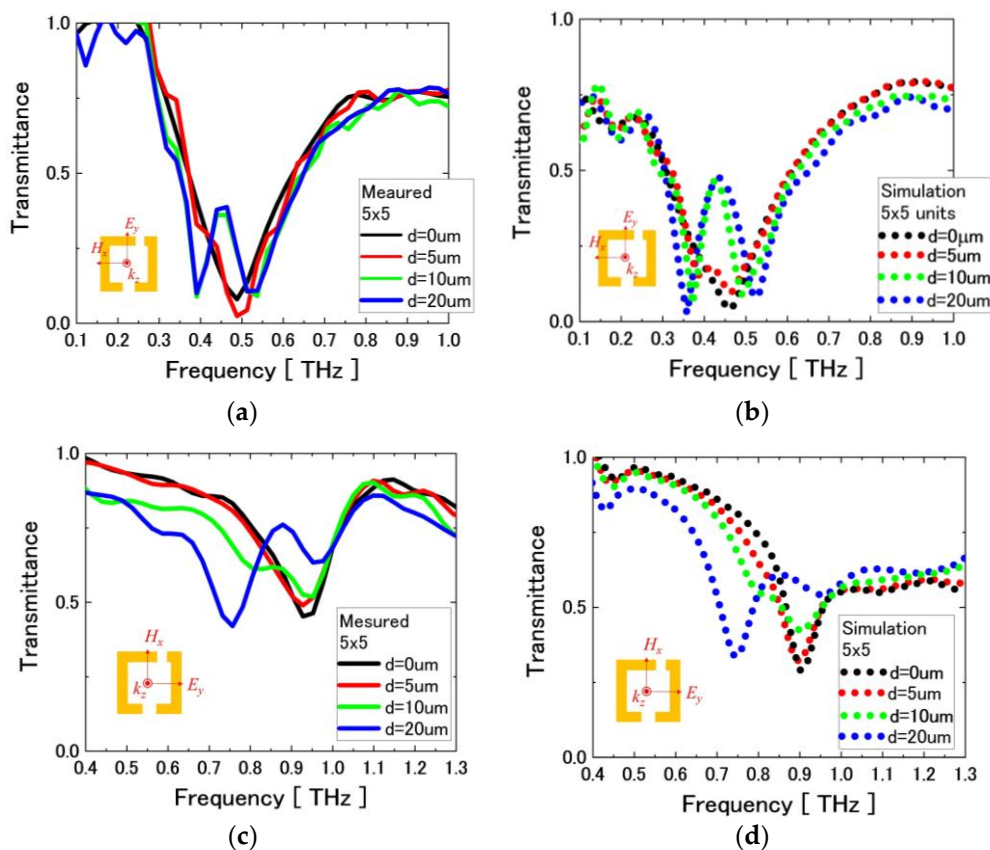


**Figure 2.** (a) The measured and (b) calculated terahertz (THz) transmittance spectra of the Fano resonance with different values of “ $d$ ”. (c) The measured and (d) calculated THz transmittance spectra of the quadrupole resonance with different values of “ $d$ ”.

Another important parameter to obtain better resonance responses in the near-field emission method is the period of the meta-atoms. This can be determined by the width of the microchannel and can help us understand the range of influence of the THz electric field from the THz source. Figure 3a,b show the simulated THz electric field distribution of the asymmetrical meta-atoms around the Fano and quadrupole resonances when the period, “ $d$ ”, and the number of meta-atoms are fixed at  $100 \mu\text{m}$ ,  $5 \times 5$  units, and  $20 \mu\text{m}$ , respectively. As can be seen in both images, the electric field from the center meta-atom strongly affects several units of its neighboring meta-atoms, while the outer meta-atoms are less affected. Note that a better electric field coupling is observed for the Fano resonance than for the quadrupole resonance. Especially for the Fano resonance, the floating capacitance around the shorter rod of the meta-atom, indicated by the red arrow in Figure 3a, shows a higher electric field compared to other areas. This indicates that we can obtain better interactions between solution samples and the THz electric field when the microchannel is fabricated along this space. This type of lattice mode has been investigated [34] and is related to the sensitivity of the chip. In conventional metamaterial studies using far-field THz wave excitation, the sensitivity of the Fano resonance is better than that of the

quadrupole resonance, despite the lower Q factor [30,35]. This may be due to the different electric field profiles around the floating capacitances. When the period of the meta-atom is increased to 180  $\mu\text{m}$ , the effects on the neighboring meta-atoms diminish for the Fano resonance, as shown in Figure 3c. This is because the meta-atom, excited with localized THz waves, becomes a power feeding point and is insufficient due to the increase in the space [34]. This preliminary investigation demonstrates the possibility of sensitive THz measurements of solutions using the proposed chip with the Fano resonance shown in Figure 1a.

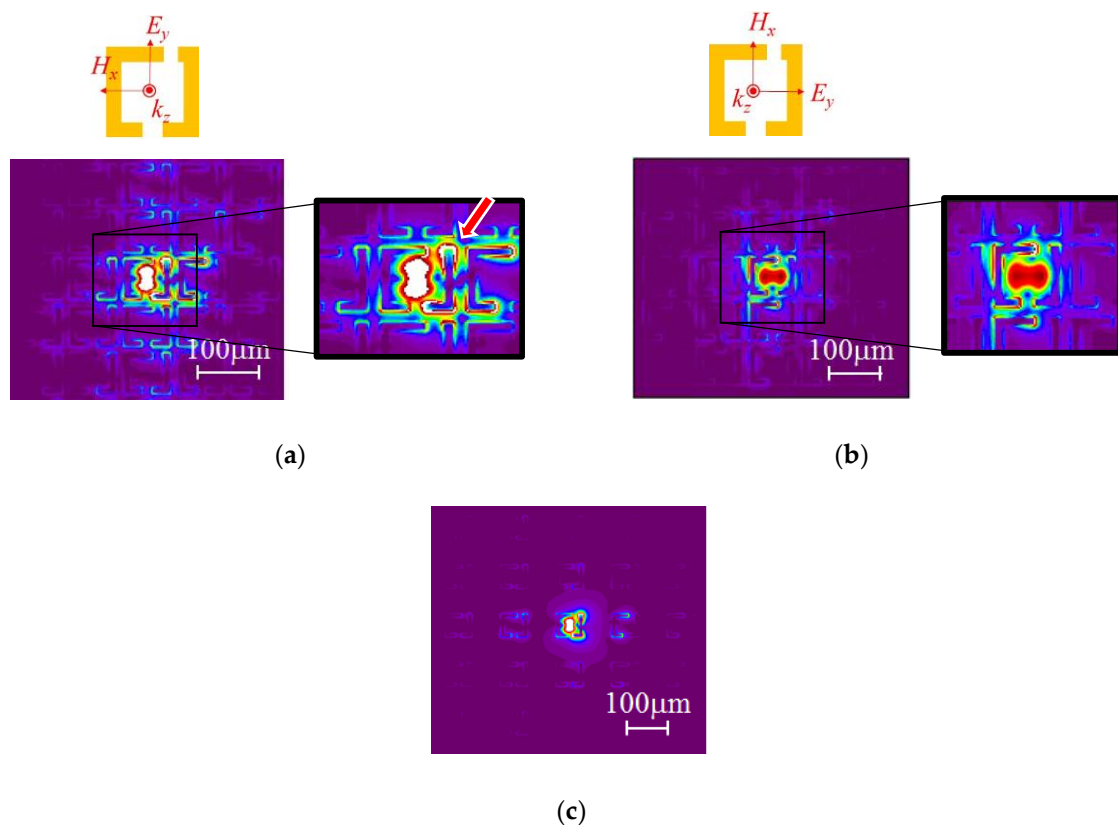


**Figure 3.** The simulated terahertz (THz) electric field distribution at the resonance frequency when the periods of the meta-atoms are (a,b) 100  $\mu\text{m}$  or (c) 180  $\mu\text{m}$ . The polarization of the THz waves is (a,c) perpendicular or (b) parallel to the gap. The number of meta-atoms is fixed at  $5 \times 5$  units for all cases.

### 3. Results and Discussion

To evaluate the chip performance, we used commercial mineral water (Contrex with 1468 mg/L of minerals) with concentrations of 0 mg/L (distilled water), 10 mg/L, and 40 mg/L as test samples. During the measurements, the channel was covered with a 580- $\mu\text{m}$ -thick quartz plate to prevent evaporation of the solution, and a solution of  $\sim 50$  nL was manually dripped using a micro-syringe (SGE0005RN) into one of the water storages that were fabricated at both sides of the channel. Then, the solution was automatically drawn into the microchannel via capillarity action and measured. After the measurement, we cleaned the chip and repeated the same process ten times, before we calculated the average THz transmittance spectra of the solution. To ensure that the chip did not hold any previous samples, we measured both the spectrum and the reflected laser image of the empty channel before each measurement. If the spectrum and the image were different from the original results, we cleaned the chip again. The actual volume of the sample calculated from the channel structure was 128 pL. All of the samples were prepared in the experimental room at 25  $^{\circ}\text{C}$  and a relative humidity of 45% before the measurements, and any drastic changes in the environment of the

experimental room were carefully avoided during the measurements. Figure 4a shows the average THz transmittance spectra of the chip with and without the solution. Note that a remarkable Fano resonance, at approximately 0.4 THz, was observed for the case of the empty chip; this was shifted to a lower frequency of approximately 0.27 THz for the case with distilled water (0 mg/L) in the microchannel. This frequency shift was due to the increase in the capacitance between the meta-atoms as a result of the substitution of the higher dielectric materials in the microchannel. In addition, the resonance frequency shifted to higher frequencies with increasing concentrations. This was due to the decrease in the refractive index of the solution in the microchannel as a result of increasing the hardness. The total shift in the resonance frequency when changing the concentration of the solution samples in the microchannel from empty to 10 mg/L was found to be approximately 130 GHz, which is a one order of magnitude improvement compared to the previous chip using symmetrical meta-atoms [29]. As a result, we confirmed that the chip operated correctly as a sensor to sensitively detect minute changes in the concentration of a solution.

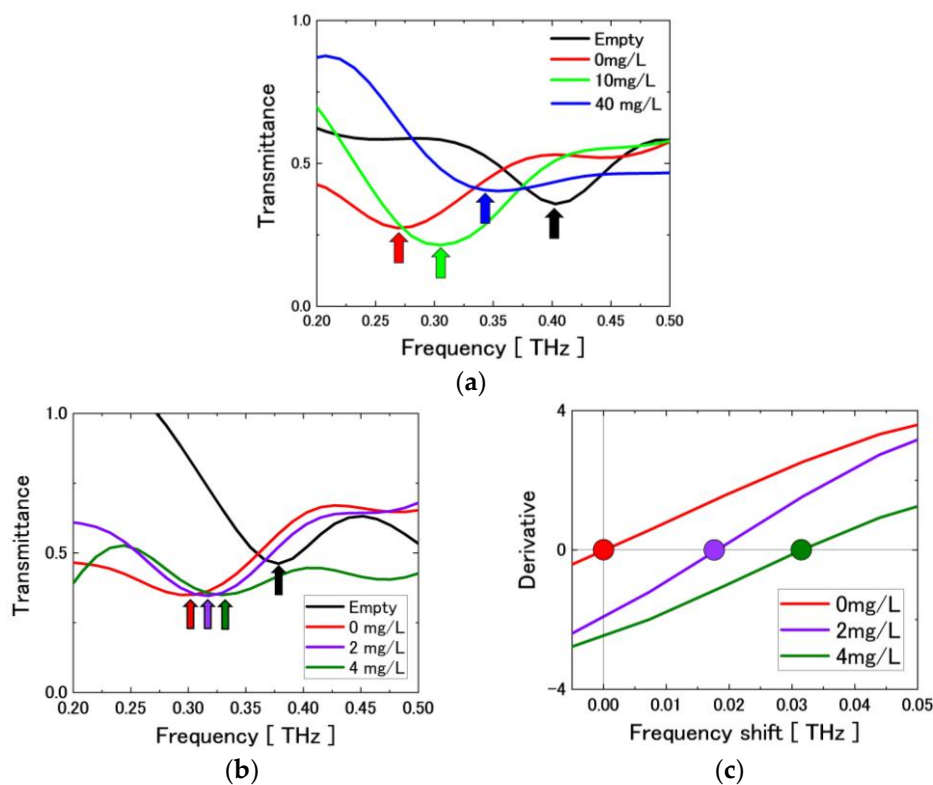


**Figure 4.** The average terahertz (THz) transmittance spectra of (a) commercial mineral water and (b) a glucose water solution at different concentrations. (c) The differential THz transmittance spectra with the deviations from the resonance frequency of the distilled water.

We also used a glucose water solution with concentrations of 0 mg/L (distilled water), 2 mg/L, and 4 mg/L and measured its resonance characteristics, as in the previous experiments, using mineral water. Figure 4b shows the average THz transmittance spectra of the three glucose water solutions with different concentrations. A similar tendency in the resonance characteristics was observed; the resonance frequency shifted slightly to higher frequencies with increasing glucose concentration. The reason for this frequency shift could be the increase in the floating capacitance between the meta-atoms through their replacement into a lower refractive index material. To further examine this frequency shift, we calculated the differential THz transmittance spectra with deviations from the resonance frequency of the distilled water, as shown in Figure 4c. We clearly observed minute changes in the concentration of the solution by monitoring the amount of shift in the resonance frequency. Because of this measurement, a maximum detectable sensitivity of 1.4 fmol of glucose was found

for a 128 pL solution. This sensitivity is an order of magnitude greater than that obtained in our previous study [29].

#### 4. Conclusions

In summary, we developed a non-linear optical crystal (NLOC)-based THz-microfluidic chip with a few arrays of asymmetrical meta-atoms to measure ultra-trace amounts of solution samples. By optimizing the structural asymmetry, as well as the periods and numbers of arrayed meta-atoms, we observed sharp Fano resonances when the central meta-atom was irradiated by localized THz waves. The chip was evaluated using commercial mineral water and a glucose water solution at different concentrations, and we were able to detect 1.4 fmol of the solute in a 128 pL solution. This sensitivity is roughly equivalent to an improvement of one order of magnitude compared to our prototype chip using symmetrical meta-atoms. Because NLOCs are relatively low-cost, such chips can be used as compact, disposable sensors in the medical and biological fields. In addition, this technique can be integrated into conventional micro-chemical chips and will accelerate the development of a THz lab-on-a-chip.

**Author Contributions:** K.S.; resources, validation, software, and writing—original draft preparation, H.M.; methodology, writing—review and editing, and I.K.; writing—review and editing, M.T.; conceptualization and supervision.

**Funding:** This work was partially supported by JSPS KAKENHI, Grant Numbers JP18H01499 and JP17H01269.

**Conflicts of Interest:** The authors declare no conflict of interest.

#### References

1. Kopp, M.U.; De Mello, A.J.; Manz, A. Chemical amplification: Continuous-flow PCR on a chip. *Science* **1998**, *280*, 1046–1048. [[CrossRef](#)] [[PubMed](#)]
2. Castillo-León, J.; Svendsen, W.E. *Lab-on-a-Chip Devices and Micro-Total Analysis Systems*; Springer: Berlin/Heidelberg, Germany, 2014.
3. Dolnik, V. DNA sequencing by capillary electrophoresis. *J. Biochem. Biophys. Methods* **1999**, *41*, 103–119. [[CrossRef](#)]
4. Liu, F.; Liu, X.; Ng, S.; Chan, H. Enantioselective molecular imprinting polymer coated QCM for the recognition of l-tryptophan. *Sens. Actuators B* **2006**, *113*, 234–240. [[CrossRef](#)]
5. Slavík, R. Homola, Ultrahigh resolution long range surface plasmon-based sensor. *J. Sens. Actuators B* **2007**, *123*, 10–12. [[CrossRef](#)]
6. Zhu, Z.; Lu, J.J.; Liu, S. Protein separation by capillary gel electrophoresis: A review. *Anal. Chim. Acta* **2012**, *709*, 21–31. [[CrossRef](#)] [[PubMed](#)]
7. Tonouchi, M. Cutting-edge terahertz technology. *Nat. Photonics* **2007**, *1*, 97–105. [[CrossRef](#)]
8. Son, J. *Terahertz Biomedical Science and Technology*; CRC Press: Boca Raton, FL, USA, 2014.
9. Heugen, U.; Schwaab, G.; Bründermann, E.; Heyden, M.; Yu, X.; Leitner, D.M.; Havenith, M. Solute-induced retardation of water dynamics probed directly by terahertz spectroscopy. *Proc. Natl. Acad. Sci. USA* **2006**, *103*, 12301–12306. [[CrossRef](#)] [[PubMed](#)]
10. Thrane, L.; Jacobsen, R.H.; Jepsen, P.U.; Keiding, S.R. THz reflection spectroscopy of liquid water. *Chem. Phys. Lett.* **1995**, *240*, 330–333. [[CrossRef](#)]
11. Jepsen, P.U.; Cooke, D.G.; Koch, M. Terahertz spectroscopy and imaging—Modern techniques and applications. *Laser Photonics Rev.* **2011**, *5*, 124–166.
12. Mittleman, D.M. Twenty years of terahertz imaging. *Opt. Express* **2018**, *26*, 9417–9431. [[CrossRef](#)]
13. Lee, D.K.; Kang, J.H.; Kwon, J.; Lee, J.S.; Lee, S.; Woo, D.H.; Kim, J.H.; Song, C.S.; Park, Q.H.; Seo, M. Nano metamaterials for ultrasensitive Terahertz biosensing. *Sci. Rep.* **2017**, *7*, 8146. [[CrossRef](#)] [[PubMed](#)]
14. Yang, X.; Wei, D.; Yan, S.; Liu, Y.; Yu, S.; Zhang, M.; Yang, Z.; Zhu, X.; Huang, Q.; Cui, H.L.; et al. Rapid and label-free detection and assessment of bacteria by terahertz time-domain spectroscopy. *J. Biophotonics* **2016**, *9*, 1050–1058. [[CrossRef](#)] [[PubMed](#)]

15. Berrier, A.; Schaafsma, M.C.; Nonglaton, G.; Bergquist, J.; Rivas, J.G. Selective detection of bacterial layers with terahertz plasmonic antennas. *Biomed. Opt. Express* **2012**, *3*, 2937–2949. [[CrossRef](#)] [[PubMed](#)]
16. Zou, Y.; Liu, Q.; Yang, X.; Huang, H.C.; Li, J.; Du, L.H.; Li, Z.R.; Zhao, J.H.; Zhu, L.G. Label-free monitoring of cell death induced by oxidative stress in living human cells using terahertz ATR spectroscopy. *Biomed. Opt. Express* **2018**, *9*, 14–24. [[CrossRef](#)] [[PubMed](#)]
17. Tang, Q.; Liang, M.; Lu, Y.; Wong, P.K.; Wilmink, G.J.; Zhang, D.D.; Xin, H. Microfluidic devices for terahertz spectroscopy of live cells toward lab-on-a-chip applications. *Sensors* **2016**, *16*, 476. [[CrossRef](#)] [[PubMed](#)]
18. Fischer, B.M.; Walther, M.; Jepsen, P.U. Far-infrared vibrational modes of DNA components studied by terahertz time-domain spectroscopy. *Phys. Med. Biol.* **2002**, *47*, 3807. [[CrossRef](#)]
19. Nagel, M.; Haring Bolivar, P.; Brucherseifer, M.; Kurz, H.; Bosserhoff, A.; Büttner, R. Integrated THz technology for label-free genetic diagnostics. *Appl. Phys. Lett.* **2002**, *80*, 154–156. [[CrossRef](#)]
20. Murakami, H.; Serita, K.; Maekawa, Y.; Fujiwara, S.; Matsuda, E.; Kim, S.; Kawayama, I.; Tonouchi, M. Scanning laser terahertz imaging system. *J. Phys. D Appl. Phys.* **2014**, *47*, 374007. [[CrossRef](#)]
21. Murakami, H.; Fujiwara, S.; Kawayama, I.; Tonouchi, M. Study of photoexcited-carrier dynamics in GaAs photoconductive switches using dynamic terahertz emission microscopy. *Photonics Res.* **2016**, *4*, A9–A15. [[CrossRef](#)]
22. Sakai, Y.; Kawayama, I.; Nakanishi, H.; Tonouchi, M. Polarization imaging of imperfect m-plane GaN surfaces. *APL Photonics* **2017**, *2*, 041304. [[CrossRef](#)]
23. Serita, K.; Mizuno, S.; Murakami, H.; Kawayama, I.; Takahashi, Y.; Yoshimura, M.; Mori, Y.; Darmo, J.; Tonouchi, M. Scanning laser terahertz near-field imaging system. *Opt. Express* **2012**, *20*, 12959–12965. [[CrossRef](#)] [[PubMed](#)]
24. Withayachumnankul, W.; Lin, H.; Serita, K.; Shah, C.; Sriram, S.; Bhaskaran, M.; Tonouchi, M.; Fumeaux, C.; Abbott, D. Sub-diffraction thin-film sensing with planar terahertz metamaterials. *Opt. Express* **2012**, *20*, 3345–3352. [[CrossRef](#)] [[PubMed](#)]
25. Serita, K.; Murakami, H.; Kawayama, I.; Takahashi, Y.; Yoshimura, M.; Mori, Y.; Tonouchi, M. Evaluation of human hairs with terahertz wave. *Opt. Eng.* **2013**, *53*, 031205. [[CrossRef](#)]
26. Fumeaux, C.; Lin, H.; Serita, K.; Withayachumnankul, W.; Kaufmann, T.; Tonouchi, M.; Abbott, D. Distributed source model for the full-wave electromagnetic simulation of nonlinear terahertz generation. *Opt. Express* **2012**, *20*, 18397–18414. [[CrossRef](#)] [[PubMed](#)]
27. Rakshit, R.; Sarkar, D.; Pal, M.; Serite, K.; Tonouchi, M.; Mandal, K. Acoustic vibration induced high electromagnetic responses of Fe<sub>3</sub>O<sub>4</sub> nano-hollow spheres in the THz regime. *J. Phys. D Appl. Phys.* **2015**, *48*, 245301. [[CrossRef](#)]
28. Kiwa, T.; Kamiya, T.; Morimoto, T.; Sakai, K.; Tsukada, K. pH measurements in 16-nL-volume solutions using terahertz chemical microscopy. *Opt. Express* **2018**, *26*, 8232–8238. [[CrossRef](#)] [[PubMed](#)]
29. Serita, K.; Matsuda, E.; Okada, K.; Murakami, H.; Kawayama, I.; Tonouchi, M. Terahertz microfluidic chips sensitivity-enhanced with a few arrays of meta-atoms. *APL Photonics* **2018**, *3*, 051603. [[CrossRef](#)]
30. Singh, R.; Cao, W.; Al-Naib, I.; Cong, L.; Withayachumnankul, W.; Zhang, W. Ultrasensitive terahertz sensing with high-Q Fano resonances in metasurfaces. *Appl. Phys. Lett.* **2014**, *105*, 171101. [[CrossRef](#)]
31. Serita, K.; Darmo, J.; Kawayama, I.; Murakami, H.; Tonouchi, M. Direct measurements of terahertz meta-atoms with near-field emission of terahertz waves. *J. Infrared Millim. Terahertz Waves* **2017**, *38*, 1107–1119. [[CrossRef](#)]
32. Withayachumnankul, W.; Abbott, D. Metamaterials in the terahertz regime. *IEEE Photonics J.* **2009**, *1*, 99–118. [[CrossRef](#)]
33. Singh, R.; Al-Naib, I.A.; Yang, Y.; Roy Chowdhury, D.; Cao, W.; Rockstuhl, C.; Ozaki, T.; Morandotti, R.; Zhang, W. Observing metamaterial induced transparency in individual Fano resonators with broken symmetry. *Appl. Phys. Lett.* **2011**, *99*, 201107. [[CrossRef](#)]

34. Chowdhury, D.R.; Singh, R.; Reiten, M.; Zhou, J.; Taylor, A.J.; O'Hara, J.F. Tailored resonator coupling for modifying the terahertz metamaterial response. *Opt. Express* **2011**, *19*, 10679–10685. [[CrossRef](#)] [[PubMed](#)]
35. Ding, C.; Jiang, L.; Wu, L.; Gao, R.; Xu, D.; Zhang, G.; Yao, J. Dual-band ultrasensitive THz sensing utilizing high quality Fano and quadrupole resonances in metamaterials. *Opt. Commun.* **2015**, *350*, 103–107. [[CrossRef](#)]



© 2019 by the authors. Licensee MDPI, Basel, Switzerland. This article is an open access article distributed under the terms and conditions of the Creative Commons Attribution (CC BY) license (<http://creativecommons.org/licenses/by/4.0/>).